

# Strain-Engineering of InAs/GaInSb Topological Insulator Towards Majorana Platform

Lingjie Du<sup>1†</sup>, Tingxin Li<sup>1, 2, 4†</sup>, Wenkai Lou<sup>3</sup>, Xingjun Wu<sup>2, 4</sup>, Xiaoxue Liu<sup>2, 4</sup>, Zhongdong Han<sup>2, 4</sup>, Chi Zhang<sup>2, 4</sup>, Gerard Sullivan<sup>5</sup>, Amal Ikhlassi<sup>5</sup>, Kai Chang<sup>3</sup>, and Rui-Rui Du<sup>1, 2, 4\*</sup>

## ABSTRACT

Creating, detecting, and manipulating Majorana fermions (MFs) in condensed matters have attracted tremendous interest due to their relevance to topological quantum computing. A single-mode MF platform combining helical edge state of a quantum spin Hall insulator (QSHI), s-wave superconductor, and magnetic insulator was proposed early on, taking advantages of the spin-polarized single-mode dispersion and the absence of non-magnetic scattering inherent in the helical states. Moreover, the edge modes may be gapped out by nearby nanoscale magnetic insulator due to the breaking of time-reversal-symmetry (TRS), localizing a pair of Majorana bound states. A major challenge towards this platform is to engineering TRS-protected and isolated QSH edge states in robust materials system. Here we show that, a new class of QSHI in strained-layer InAs/GaInSb can be tailored by molecular beam epitaxy (MBE), with the bulk gaps being enhanced by up to five folds as compared to the binary InAs/GaSb QSHI. Remarkably, with increasing edge velocity, the edge conductance at zero and applied magnetic fields manifests TRS-protected properties conforming to the predictions of the Bernevig-Hughes-Zhang model. The InAs/GaInSb bilayers offer a much sought-after building block for the MF platform.

<sup>†</sup> These authors contributed equally to the project

\* Correspondent author: Rui-Rui Du at [rrd@rice.edu](mailto:rrd@rice.edu)

<sup>1</sup>Department of Physics and Astronomy, Rice University, Houston, Texas 77251-1892, USA

<sup>2</sup>International Center for Quantum Materials, School of Physics, Peking University, Beijing 100871, China

<sup>3</sup>SKLSM, Institute of Semiconductors, Chinese Academy of Sciences, Beijing 100083, China

<sup>4</sup>Collaborative Innovation Center of Quantum Matter, Beijing 100871, China

<sup>5</sup>Teledyne Scientific and Imaging, Thousand Oaks, California 91603, USA

## Introduction

TRS protected QSHI is a two-dimensional topological insulator<sup>1-4</sup> with a topological number  $Z_2$ . The transport evidence for quantum spin Hall effect was first observed<sup>5</sup> in HgTe/CdTe quantum well (QW) with its edge conductance quantized to the theoretical value. To date the leading materials systems are made of semiconductor QWs, *i.e.*, HgTe/CdTe QW and inverted InAs/GaSb QWs; both are described by the Bernevig-Hughes-Zhang model<sup>4</sup>. In InAs/GaSb QWs, wave-function hybridization between InAs and GaSb layers dominates the bulk and opens a minigap  $\Delta$ <sup>6</sup>, while a Kramer's pair of spin-momentum-locked edge states emerges on the device perimeters<sup>7</sup>. Relevant experiments are reported in refs<sup>8-17</sup>. The charge transport in helical edges is dissipationless, owing to the notion that the helical property prevents charge backscattering. On the other hand, theories<sup>18-20</sup> taking into account electron-electron interactions and correlations suggest that certain many-body scattering processes may exist, which should lead to dissipation.

In the inverted InAs/GaSb bilayer system, the ground electron sub-band in InAs well and the ground hole sub-band in GaSb well cross at some wave-vector  $k_{\text{cross}}$ . Spatially separated electrons and holes are strongly coupled at this crossing point due to the tunneling between two wells; consequently, a hybridization gap  $\Delta$  is opened at  $k_{\text{cross}}$ , which is the bulk gap of the QSHI. The density of the charge neutral point (CNP) in the inverted regime is referred to as  $n_{\text{cross}} = k_{\text{cross}}^2 / 2\pi$ . The degree of band inversion can be tuned by QW widths and gate voltages<sup>6,8-16</sup>, and it has dramatic influences on the bulk transport properties. In the deeply inverted regime, where typically  $n_{\text{cross}}$  above  $3 \times 10^{11} \text{ cm}^{-2}$  there always exist considerable residual states in the hybridization gap thus the bulk of InAs/GaSb QWs is not truly insulating<sup>8,9,12,13</sup>, which limits the studies and applications of helical edge states.

On the other hand, in the shallowly inverted regime ( $n_{\text{cross}}$  below  $1 \times 10^{11} \text{ cm}^{-2}$ ), the bulk is insulating to a high degree and quantized helical edge conductance plateaus were observed<sup>10,15</sup>. Surprisingly, the quantized conductance plateaus persist under external magnetic fields, in contrast with the theoretical expectations for TRS protected helical edge states<sup>10</sup>. On a general ground, Coulomb interactions of electron-hole pairs dominate over hybridization effects in

such dilute limit<sup>21</sup>, the possibility of an 2D excitonic ground state may be considered<sup>21-23</sup>. Moreover, here the edge Fermi velocity  $v_F \sim \Delta/k_{\text{cross}}$  is unusually small, in the range of  $\sim 2 \times 10^4 \text{ ms}^{-1}$  to  $\sim 5 \times 10^4 \text{ ms}^{-1}$ , indicating that the edge states are in a strongly interacting regime<sup>18-20,24</sup>. Overall, while the quantized edge transport has been observed in micrometer size samples of shallowly inverted InAs/GaSb, the resilience to external magnetic field and the observed length dependence in long samples are not account for by single-particle model. From an experimental perspective, it is much desirable to develop a plain vanilla QSHI with properties dominated by single-particle physics. Ideally, to some degree the interaction effects may be set in by tuning experimental parameters such as  $v_F$ .

In this article, we show that TRS protected QSHI has been achieved in strained-layer InAs/GaInSb QWs by alloying indium in the GaSb layer. Due to the band structural changes from strain effect, QWs can be made narrower, leading to stronger overlaps between electron and hole wave functions. This effect results in insulating hybridization gaps at low temperatures even when the  $n_{\text{cross}}$  is larger than  $3 \times 10^{11} \text{ cm}^{-2}$ . In addition, the helical edge conductance decreases under both perpendicular and in-plane magnetic fields, indicating the opening of mass gaps in the edge states. Remarkably, we found that the edge conductance and the magnetic response are correlated with  $v_F$ , which could be well controlled by lattice strain and the gate voltages. This finding opens the door for building robust single-mode MF platform supporting Majorana bound states, as well as parafermion states, for future topological quantum computing circuits<sup>25-30</sup>.

### Strain effect in InAs/GaInSb

InAs/GaSb type-II superlattice (SL) infrared detectors have been known to possess two prominent advantages over other materials: (1) InAs and GaSb has approximately the same lattice constant of 6.1 Å, thus high quality SL structure could be grown by MBE; (2) Due to the broken-gap band alignment, the energy gap of InAs/GaSb system can be well controlled by adjusting the layer width of the SL. However, it was realized that for the thicker layer SL required to reach long-wavelength sensitivity, the overlap between the wave-functions of electrons and holes is small, leading to low optical absorption efficiency. A clever way to solve

this problem is to make strained-layer InAs/Ga<sub>1-x</sub>In<sub>x</sub>Sb SL by alloying GaSb with InSb (lattice constant about 6.4 Å), proposed<sup>31</sup> by Smith and Maiholt in 1987. Because of the strain in the growth plane, the energy of the conduction band (CB) in InAs shift downward while the energy level of valence band (VB) in GaInSb splits into heavy hole (HH) level and light hole (LL) level, respectively, where the energy of the HH level is higher than the original top VB in GaSb. As a result, to reach a fixed energy band gap, the layers of InAs/GaInSb SL are made narrower than InAs/GaSb SL thereby increasing the optical absorption efficiency. Such strain-engineering has led to the invention of high-performance long-wave length SL infrared detectors<sup>32</sup>.

Similar physics idea may guide the construction of a large-gap QSHI. Based on the strain effects described above, we can reach the same inverted band structure with narrower QWs in strained-layer InAs/GaInSb, comparing to unstrained InAs/GaSb. The hybridization-induced gap should increase in such narrower QWs since the coupling between electrons and holes is now stronger. In addition, due to the energy splitting of the HH and LH in GaInSb, the Fermi surface of electrons would better match with the Fermi surface of holes, which also help to reduce the residual non-hybridized carriers.

The MBE-wafer we used for present transport measurements consists of InAs/Ga<sub>0.75</sub>In<sub>0.25</sub>Sb QWs. The thickness of InAs QW is 9.5 nm while the thickness of Ga<sub>0.75</sub>In<sub>0.25</sub>Sb QW is 4 nm, as shown in Fig. 1B. Fig. 1C shows the calculated band structure of the wafer by 8-band Kane model, with a hybridization gap  $\sim$  12 meV, which is about three-fold increases from the value  $\sim$  4 meV in unstrained InAs/GaSb QWs. Fig. 1D is a transmission electron microscope (TEM) photograph of an InAs/Ga<sub>0.68</sub>In<sub>0.32</sub>Sb wafer; it shows that the crystalline structure remains coherent across the heterostructure interfaces regardless of  $\sim$  1.2 % in-plane strain. Well resolved Shubnikov-de Haas (SdH) oscillations have been observed in both the electron regime and the hole regime (see Supplementary Fig. S2).

### Transport properties of bulk states in strained-layer InAs/GaInSb QWs

To directly measure the bulk conductance, we fabricate dual-gated Corbino devices. In this case, the edge conductance is shunted and has no contribution to the signals. Fig. 2 shows the

traces of the conductance per square  $G$  versus front-gate voltage  $V_{\text{front}}$  at base temperature  $T \sim 20$  mK with back gate voltage  $V_{\text{back}} = 0$  V and  $V_{\text{back}} = 4$  V, respectively. At the CNP, the conductance show dips, indicating the entrance into an energy gap. For more positive  $V_{\text{back}}$ , the bulk band becomes more inverted, resulting in a less insulating bulk. Nevertheless, the bulk conductance is still negligible at low temperature, about  $100$  M $\Omega$  per square at  $20$  mK for the  $V_{\text{back}} = 0$  V case, and about  $25$  M $\Omega$  per square at  $20$  mK for the  $V_{\text{back}} = 4$  V case.

Electron-hole hybridization are most favored when the Fermi momentum of electrons  $k^e_F$  and holes  $k^h_F$  are equal. Under in-plane magnetic field  $B_{\parallel}$ , applied along  $x$  axis of the example, Lorenz force gives tunneling carriers additional momentum along  $y$  axis, resulting in a relative shift of band dispersions  $\Delta k_y = -eB\Delta\langle z \rangle/h$ , (tunneling distance  $\Delta\langle z \rangle$  is limited by one-half thickness of the QWs). Consequently, carrier hybridization is suppressed due to momentum-mismatch, rendering the QWs as a bilayer-semimetal. As shown in Fig. 2A and 2B, the insulating gap at CNP is gradually closed with the increasing  $B_{\parallel}$ , which agrees with the behavior of a hybridization gap under in-plane magnetic field, but in contrast with the behavior of the insulating exciton gap observed in shallowly-inverted InAs/GaSb QW<sup>23</sup>. Hybridization gaps with residual conductivity have been commonly reported<sup>6,8,12,13</sup>; this is the first time that a truly insulating hybridization gap is observed at low temperature.

Under perpendicular magnetic field  $B_{\perp}$ , the bulk becomes more insulating due to localization effects, as shown in Fig. 2C and 2D. Fig. 2E shows the Arrhenius plots of a Corbino device made of strained-layer InAs/Ga<sub>0.75</sub>In<sub>0.25</sub>Sb QWs and a Corbino device made of shallowly inverted InAs/GaSb QWs (data adapted from Ref. 10 at  $B = 0$  T). The shallowly-inverted InAs/GaSb QWs shows an insulating gap  $\sim 26$ K at lower temperatures, which, presumably, associate with the formation of an exciton insulator<sup>23</sup>. Although the bulk conductance is suppressed at low temperature ( $< 300$  mK, see Supplementary Fig. S3) for the InAs/Ga<sub>0.75</sub>In<sub>0.25</sub>Sb QWs, it lacks the exponential dependences characterizing an exciton insulator; the transport in this regime is more like variable-range hopping. Indeed, here the CNP density ranges from  $\sim 2 \times 10^{11}$  cm<sup>-2</sup> to  $\sim 3 \times 10^{11}$  cm<sup>-2</sup>, substantially above the onset of exciton insulator  $\sim 1 \times 10^{11}$  cm<sup>-2</sup> as discussed in ref. 23. At higher temperatures, the hybridization gap values can be roughly determined by fitting the Arrhenius plots, which is

~ 66 K for the shallowly inverted InAs/GaSb QWs, and ~ 130 K for the InAs/Ga<sub>0.75</sub>In<sub>0.25</sub>Sb QWs. Overall, a larger hybridization gap has been achieved by strain-engineering, in reasonable agreement with the calculations.

### Controllable helical edge states with long characteristic length

We now turn to the helical edge properties of strained-layer InAs/Ga<sub>0.75</sub>In<sub>0.25</sub>Sb QWs. Fig. 3A shows the longitudinal resistance  $R_{xx}$ - $V_{\text{front}}$  traces of a 100  $\mu\text{m} \times 50 \mu\text{m}$  Hall bar device with various  $V_{\text{back}}$  at  $T \sim 20 \text{ mK}$ . Here the measured  $R_{xx}$  is solely resulted from the edge channels, since the bulk is fully insulating at such low  $T$ . At  $V_{\text{back}} = 0 \text{ V}$ , the resistance peak is about 115 k $\Omega$ , corresponding to a characteristic length  $\lambda_\varphi$  (refers to a length scale at which dissipationless edge transport breaks down and counter propagating spin-up and spin-down channels equilibrate) about 11  $\mu\text{m}$ . The  $\lambda_\varphi$  of different devices made by this wafer mostly range from 5  $\mu\text{m}$  to 10  $\mu\text{m}$ , significantly longer than those in previous studies<sup>5,10</sup> of the QSHI. Very surprisingly, the  $\lambda_\varphi$  can be tuned by gate: as shown in Fig. 3A the resistance peak values gradually decreases with decreasing  $V_{\text{back}}$  (namely, less inverted), indicating that the  $\lambda_\varphi$  increase from ~ 6  $\mu\text{m}$  at  $V_{\text{back}} = 4 \text{ V}$  to ~ 11  $\mu\text{m}$  at  $V_{\text{back}} = 0 \text{ V}$ . (Note for this device the backgate bias was limited within 4V and 0V). The insets of Fig. 3A illustrate the  $\lambda_\varphi$  and the  $n_{\text{cross}}$  (deduced from magneto-transport data) versus  $V_{\text{back}}$ .

According to the definition of characteristic length, if the device edge length is shorter than  $\lambda_\varphi$ , the edge conductance measured should be quantized to  $2e^2/h$ . This is indeed confirmed in a Hall bar device of length 10  $\mu\text{m}$ , as shown in Fig. 3B. As the  $\lambda_\varphi$  is being tuned from 6  $\mu\text{m}$  to 11  $\mu\text{m}$ , the  $R_{xx}$  decreases, and finally reaches a plateau of 12.9 k $\Omega$  with reasonable accuracy.

A plausible explanation for above data is related to the interaction effects<sup>18-20</sup> in the helical edge state. At more positive  $V_{\text{back}}$ , the bulk band becomes more inverted hence a larger  $k_{\text{cross}}$  and a roughly constant  $\Delta^7$ , overall this would lead to a smaller Fermi velocity  $v_F \sim \Delta/k_{\text{cross}}$  of the helical edge states, resulting in more prominent interaction effects for the edge electrons. The backscattering processes would enhance when the electron-electron interactions become stronger, thus the helical edge states exhibit a shorter characteristic length in the more inverted case.

## TRS protected helical edge states

In general, applying magnetic field will break the TRS and open a gap in the helical edge states. 1D massless Dirac fermion could be tuned into 1D massive fermion allowing for backscattering, thereby the helical edge resistance will increase (Fig.1A). However, in previous studies<sup>10</sup> of shallowly inverted InAs/GaSb QWs, regardless of that an insulating bulk and quantized helical edge conductance had been observed, the quantized conductance plateaus persist under external magnetic fields, in contrast with the theoretical expectations for TRS protected helical edge states.

Remarkably, for all devices made by strained-layer InAs/Ga<sub>0.75</sub>In<sub>0.25</sub>Sb QWs, the helical edge conductance show clear magnetic field dependence. Specifically, for a 3  $\mu\text{m} \times 1.5 \mu\text{m}$  Hall bar device, it shows quantized resistance plateau of  $h/2e^2$  at zero magnetic field, as shown in Fig 4A and 4B. Under a perpendicular magnetic field, as shown in Fig. 4A, the plateau values ( $R_{\text{CNP}}$ ) increase at first ( $B_{\perp}$  below 5 T) due to TRS breaking, then decrease at higher  $B_{\perp}$ , indicating the edge states undergoing a transition from helical edge states to chiral edge states. For a long sample of 100  $\mu\text{m} \times 50 \mu\text{m}$  Hall bar, the helical edge resistance also increases under  $B_{\perp}$ , as shown in Fig. 4C and 4D. The response to an in-plane field shows an interesting behavior. Under a small in-plane magnetic field up to 3 T (Fig. 4B), the measured resistance of the 3  $\mu\text{m} \times 1.5 \mu\text{m}$  Hall bar increases due to TRS breaking. For  $B_{\parallel}$  above 3 T, we observed that the sample resistance decreases with  $B_{\parallel}$ , primarily because the bulk becomes conductive under higher  $B_{\parallel}$  (see Supplementary Fig. S4 and S5).

## Discussion on Luttinger parameter $K$

One of the most attractive features of the strained-layer InAs/GaInSb system is the relatively large hybridization gap, and the gap size can be well controlled by the strain of the QWs. By using 8-band Kane model, the calculated hybridization gap can be as large as  $\sim 20$  meV with increasing indium fractions. A larger hybridization gap leads to an increasing edge  $v_F$ . Electron-electron interaction effects in the helical edge can be parameterize by  $K$ , and  $K$  is strongly correlated with  $v_F$  and other factors such as screening from the environment<sup>19,20</sup>. In

general, the helical Luttinger liquid has several fix points in the axis of  $K$ , namely,  $K = 1$ ,  $K = 1/2$ , and  $K = 1/4$ . In a recent measurement for helical edge states in (regular) InAs/GaSb QWs, for  $v_F \sim 5 \times 10^4 \text{ ms}^{-1}$ , we have determined  $K \sim 0.22$ , which is close to  $1/4$ . The edge transport in ultralow temperatures shows strong helical Luttinger-liquid behavior as evidenced by a distinct signature of conductivity scaling in  $(eV/k_B T)$ .

As for the strained-layer InAs/GaInSb system, if we adopt a hybridization gap  $\sim 20 \text{ meV}$ , screening length  $\sim 50 \text{ nm}$ , QWs width  $\sim 12 \text{ nm}$ , and  $n_{\text{cross}}$  from  $1 \times 10^{11} \text{ cm}^{-2}$  to  $2 \times 10^{11} \text{ cm}^{-2}$ , then the estimated  $v_F$  of helical edge states ranges from  $\sim 1.3 \times 10^5 \text{ m}^{-1}$  to  $\sim 1.9 \times 10^5 \text{ m}^{-1}$ , and consequently the  $K$  value from  $\sim 0.43$  to  $0.5$ . Thus even without further refining, the present system should cover the range of  $1/4$  (strongly-interacting) through  $1/2$  (weakly-interacting) in Luttinger parameter.

Returning to the MF platform, a profound prospect that this new class of QSHI can bring in is the engineering of parafermionic states<sup>33-34</sup> arising in superconductor proximity-coupled interacting helical edges, which would go beyond the MF paradigm made of non-interacting 1D modes, promising for universal decoherence-free quantum computation. A defining characteristic of parafermions is  $8\pi$ -periodic Josephson effect<sup>33-34</sup>. Note that although detecting localized parafermionic zero modes in a SC/QSHI/SC Josephson junction require strong interactions in the helical edge state, the striking  $8\pi$ -periodic Josephson effect can survive even in the weakly interacting regime.

## Summary

By strain-engineering, we have realized for the first time a TRS protected QSHI in InAs/GaInSb QWs, which shows a larger hybridization gap and longer characteristic length than previous QSHI systems. Moreover, the bulk is enough insulating at low temperatures and the edge characteristic length may be well controlled by the gates; data shows that the edge states can be gapped out by applying magnetic fields. Our findings not only provide a nearly idea system for creating, detecting, and manipulating MFs, but also move one step closer to the device and circuit applications of QSHI based on semiconductor technology.

## **Acknowledgments**

We thank Carlo Beenakker, Xincheng Xie, and Shoucheng Zhang for helpful discussions. The work at Rice were supported by NSF Grants No. DMR-1508644 and Welch Foundation Grants No. C-1682, work at PKU were supported by National Basic Research Program of China Grants No. 2014CB920901, work at IoS, CAS were supported by NSFC Grants No. 11434010 and National Basic Research Program of China Grants No. 2015CB921503.

## **Author Contributions**

LJD and TXL fabricated devices and made measurements, WKL and KC calculated band structures, GS and AI grew the wafers, XJW, XXL, ZDH, and CZ assisted in experiments, LJD, TXL, and RRD analyzed data and wrote the manuscript, RRD conceived and supervised the project.

## **Additional information**

Supplementary Information is linked to the online version of the paper. Correspondence and requests for materials should be addressed to R.R.D. ([rrd@rice.edu](mailto:rrd@rice.edu)).

## Figure Captions

**Figure 1 | Illustration of a single-mode Majorana platform based on proximity-coupled strain-layer quantum spin Hall insulator.** **(A)** Left panel: Schematic drawing for detecting MFs in strained InAs/GaInSb QWs. Since the lattice constant of GaInSb is larger than that of InAs, the GaInSb lattice is compressed and the InAs lattice is under tension. Superconductors and magnetic insulators are used for opening superconductor gap and the mass gap at the helical edge states, respectively. Right panel: Schematic drawing of band dispersion in InAs/GaInSb QWs, the edge  $v_F$  is proportional to  $\Delta/k_{\text{cross}}$ . **(B)** Wafer structures of the strained-layer InAs/Ga<sub>0.75</sub>In<sub>0.25</sub>Sb QWs used for experiments. **(C)** Calculated band structure of the 9.5 nm InAs/ 4nm Ga<sub>0.75</sub>In<sub>0.25</sub>Sb QWs, CB1, VB1 and CB2, VB2 represent for different spin component. **(D)** A TEM photograph of a strained InAs/Ga<sub>0.68</sub>In<sub>0.32</sub>Sb wafer; blue and red lines are guide for eyes.

**Figure 2 | Transport data of bulk states from Corbino devices.**  $G$ - $V_{\text{front}}$  traces under 0 T, 4 T, 6 T, 8 T, 12 T, and 18 T in-plane magnetic field at **(A)**  $V_{\text{back}} = 0$  V and **(B)**  $V_{\text{back}} = 4$  V.  $G$ - $V_{\text{front}}$  traces under 0 T, 1 T, 2 T, 3 T, and 4 T perpendicular magnetic field at **(C)**  $V_{\text{back}} = 0$  V and **(D)**  $V_{\text{back}} = 4$  V. **(A)-(D)** measured at  $T \sim 20$  mK. **(E)** Arrhenius plots for strained-layer InAs/Ga<sub>0.75</sub>In<sub>0.25</sub>Sb QWs (black squares), and unstrained 12.5 nm InAs/10 nm GaSb QWs (red cycles). Energy gaps can be deduced by fitting  $G_{xx} \propto \exp(-\Delta/2k_B T)$ , as shown by straight dash lines in the plot.

**Figure 3 | Helical edge transport in strained-layer InAs/Ga<sub>0.75</sub>In<sub>0.25</sub>Sb QWs.**  $R_{\text{xx}}$ - $V_{\text{front}}$  traces measured from **(A)** a 100  $\mu\text{m} \times 50 \mu\text{m}$  Hall bar device and **(B)** a 10  $\mu\text{m} \times 5 \mu\text{m}$  Hall bar device at  $T \sim 20$  mK with  $V_{\text{back}} = 0$  V, 1V, 2 V, 3 V, and 4 V. The edge coherence length increase with decreasing  $V_{\text{back}}$ . The inset in **(A)** shows the  $\lambda_\varphi$  and the  $n_{\text{cross}}$  values as the change of  $V_{\text{back}}$ .

**Figure 4 | Helical edge conductance under magnetic field.** **(A)**  $R_{\text{xx}}$ - $V_{\text{front}}$  traces of a 3  $\mu\text{m} \times 1.5 \mu\text{m}$  Hall bar under different perpendicular magnetic field ( $V_{\text{back}} = 0$  V). Inset in **(A)**, the  $R_{\text{CNP}}$  values increase when  $B_\perp < 5$  T, indicating that backscattering processes began to occur in the helical edge due to TRS breaking. At higher  $B_\perp$ ,  $R_{\text{CNP}}$  began to decrease, since the magnetic field would push the edge states of one chirality outward and the opposite chirality

inward. **(B)**  $R_{xx}$ - $V_{\text{front}}$  traces of the  $3 \mu\text{m} \times 1.5 \mu\text{m}$  Hall bar under different in-plane magnetic field. The resistance plateau values also beyond the quantized value under  $B_{\parallel}$  because of TRS breaking.  $R_{xx}$ - $V_{\text{front}}$  traces of the  $100 \mu\text{m} \times 50 \mu\text{m}$  Hall bar under different perpendicular magnetic field at **(C)**  $V_{\text{back}} = 0 \text{ V}$  and **(D)**  $V_{\text{back}} = 4 \text{ V}$ .

## Reference

1. M. Z. Hasan, C. L. Kane, Colloquium: Topological insulators. *Rev. Mod. Phys.* **82**, 3045-3067 (2010).
2. X. L. Qi, S. C. Zhang, Topological insulator and superconductors. *Rev. Mod. Phys.* **83**, 1057-1110 (2011).
3. C. L. Kane, E. J. Mele,  $Z_2$  topological order and the quantum spin Hall effect. *Phys. Rev. Lett.* **95**, 146802 (2005).
4. B. A. Bernevig, T. L. Hughes, S. C. Zhang, Quantum spin Hall effect and topological phase transition in HgTe quantum wells. *Science* **314**, 1757-1761 (2006).
5. M. König, S. Wiedmann, C. Brüne, A. Roth, H. Buhmann, L. W. Molenkamp, X. L. Qi, S. C. Zhang, Quantum spin Hall insulator state in HgTe quantum wells. *Science* **318**, 766-770 (2007).
6. M. J. Yang, C. H. Yang, B. R. Bennett, B. V. Shanabrook, Evidence of a hybridization gap in “semimetallic” InAs/GaSb Systems. *Phys. Rev. Lett.* **78**, 4613-4616 (1997).
7. C. X. Liu, T. L. Hughes, X. L. Qi, K. Wang, S. C. Zhang, Quantum spin Hall effect in inverted type-II semiconductors. *Phys. Rev. Lett.* **100**, 236601 (2008).
8. I. Knez, R. R. Du, G. Sullivan, Finite conductivity in mesoscopic Hall bars of inverted InAs/GaSb quantum wells. *Phys. Rev. B* **81**, 201301(R) (2010).
9. I. Knez, R. R. Du, G. Sullivan. Evidence for helical edge modes in inverted InAs/GaSb quantum wells. *Phys. Rev. Lett.* **107**, 136603 (2011).
10. L. Du, I. Knez, G. Sullivan, R. R. Du, Robust helical edge transport in gated InAs/GaSb bilayers. *Phys. Rev. Lett.* **114**, 096802 (2015).
11. W. Pan, J. F. Klem, J. K. Kim, M. Thalakulam, M. J. Cich, S. K. Lyo, Chaotic quantum transport near the charge neutrality point in inverted type-II InAs/GaSb field-effect transistors. *Appl. Phys. Lett.* **102**, 033504 (2013).
12. K. Suzuki, Y. Harada, K. Onomitsu, K. Muraki, Gate-controlled semimetal-topological insulator transition in an InAs/GaSb heterostructure. *Phys. Rev. B* **91**, 245309 (2015).
13. S. Mueller, A. N. Pal, M. Karalic, T. Tschirky, C. Charpentier, W. Wegscheider, K. Ensslin, T. Ihn, Nonlocal transport via edge states in InAs/GaSb coupled quantum wells. *Phys. Rev. B* **92**, 081303(R) (2015).
14. F. Qu, A. J. A. Beukman, S. Nadj-Perge, M. Wimmer, B. M. Nguyen, W. Yi, J. Thorp, M. Sokolich, A. A. Kiselev, M. J. Manfra, C. M. Marcus, L. P. Kouwenhoven, Electric and magnetic tuning between the trivial and topological phases in InAs/GaSb double quantum wells. *Phys. Rev. Lett.* **115**, 036803 (2015).
15. F. Couëdo, H. Irie, K. Suzuki, K. Onomitsu, K. Muraki, Single-edge transport in an InAs/GaSb quantum spin Hall insulator. *Phys. Rev. B* **94**, 035301 (2016).

16. F. Nichele, H. J. Suominen, M. Kjaergaard, C. M. Marcus, E. Sajadi, J. A. Folk, F. Qu, A. J. A. Beukman, F. K. de Vries, Edge transport in the trivial phase of InAs/GaSb. *New J. Phys.* **18**, 083005 (2016).

17. B. M. Nguyen, A. A. Kiselev, R. Noah, W. Yi, F. Qu, A. J. A. Beukman, F. K. de Vries, J. van Veen, S. Nadj-Perge, L. P. Kouwenhoven, M. Kjaergaard, H. J. Suominen, F. Nichele, C. M. Marcus, M. J. Manfra, M. Sokolich, Decoupling Edge Versus Bulk Conductance in the Trivial Regime of an InAs/GaSb Double Quantum Well Using Corbino Ring Geometry. *Phys. Rev. Lett.* **117**, 077701 (2016).

18. C. Wu, B. A. Bernevig, S. C. Zhang, Helical liquid and the edge of quantum spin Hall systems. *Phys. Rev. Lett.* **96**, 106401 (2006).

19. J. C. Y. Teo, C. L. Kane. Critical behavior of a point contact in a quantum spin Hall insulator. *Phys. Rev. B* **79**, 235321 (2009).

20. J. Maciejko, C. Liu, Y. Oreg, X. L. Qi, C. Wu, S. C. Zhang. Kondo Effect in the Helical Edge Liquid of the Quantum Spin Hall State. *Phys. Rev. Lett.* **102**, 256803 (2009).

21. Y. Naveh and B. Laikhtman, Excitonic Instability and Electric-Field-Induced Phase Transition Towards a Two-Dimensional Exciton Condensate. *Phys. Rev. Lett.* **77**, 900 (1996).

22. D. I. Pikulin, T. Hyart, Interplay of Exciton Condensation and the Quantum Spin Hall Effect in InAs/GaSb Bilayers. *Phys. Rev. Lett.* **112**, 176403 (2014).

23. L. Du, W. Lou, K. Chang, G. Sullivan, R. R. Du, Gate-tuned spontaneous exciton insulator in double-quantum wells. arXiv: 1508.04509.

24. T. Li, P. Wang, H. Fu, L. Du, K. A. Schreiber, X. Mu, X. Liu, G. Sullivan, G. A. Csáthy, X. Lin, R. R. Du, Observation of a helical Luttinger liquid in InAs/GaSb quantum spin Hall edges. *Phys. Rev. Lett.* **115**, 136804 (2015).

25. J. Alicea, Exotic matter: Majorana modes materialize. *Nature Nanotechnology* **8**, 623-624 (2013).

26. J. Alicea, New directions in the pursuit of Majorana fermions in solid state systems. *Rep. Prog. Phys.* **75**, 076501 (2012).

27. C. W. J. Beenakker, Search for Majorana fermions in superconductors. *Annu. Rev. Condens. Matter Phys.* **4**, 113-136 (2013).

28. J. Nilsson, A. R. Akhmerov, C. W. J. Beenakker, Splitting of a Cooper pair by a pair of Majorana bound states. *Phys. Rev. Lett.* **101**, 120403 (2008).

29. L. Fu, C. L. Kane, Josephson current and noise at a superconductor/ quantum-spin-Hall-insulator /superconductor junction. *Phys. Rev. B* **79**, 161408(R) (2009).

30. S. Mi, D. I. Pikulin, M. Wimmer, C. W. J. Beenakker, Proposal for the detection and braiding of Majorana fermions in a quantum spin Hall insulator. *Phys. Rev. B* **87**, 241405(R) (2013).

31. D. L. Smith, C. Mailhiot, Proposal for strained type II superlattice infrared detectors. *J.*

*Appl. Phys.* **62**, 2545-2548 (1987).

32. F. Fuchs, U. Weimer, W. Pletschen, J. Schmitz, E. Ahlswede, M. Walther, J. Wagner, P. Koidl, High performance InAs/Ga<sub>1-x</sub>In<sub>x</sub>Sb superlattice infrared photodiodes. *Appl. Phys. Lett.* **71**, 3251-3253 (1997).

33. F. Zhang, C. L. Kane, Time-Reversal-Invariant Z<sub>4</sub> Fractional Josephson Effect. *Phys. Rev. Lett.* **113**, 036401 (2014).

34. C. P. Orth, R. P. Tiwari, T. Meng, T. L. Schmidt. Non-Abelian parafermions in time-reversal-invariant interacting helical systems. *Phys. Rev. B* **91**, 081406(R) (2015).

35. J. Alicea, P. Fendley, Topological Phases with Parafermions: Theory and Blueprints. *Annu. Rev. Condens. Matter Phys.* **7**, 119-139 (2016).

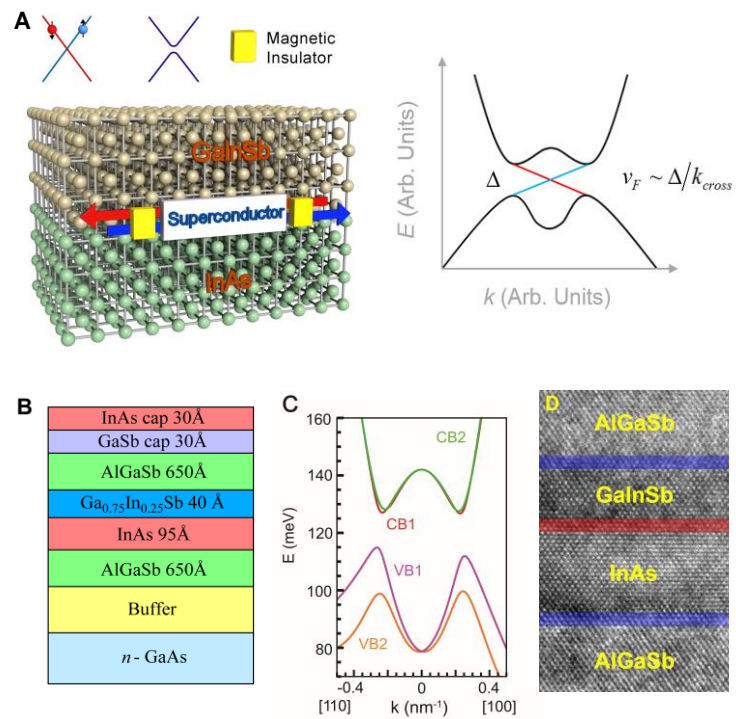


**Figure 1**

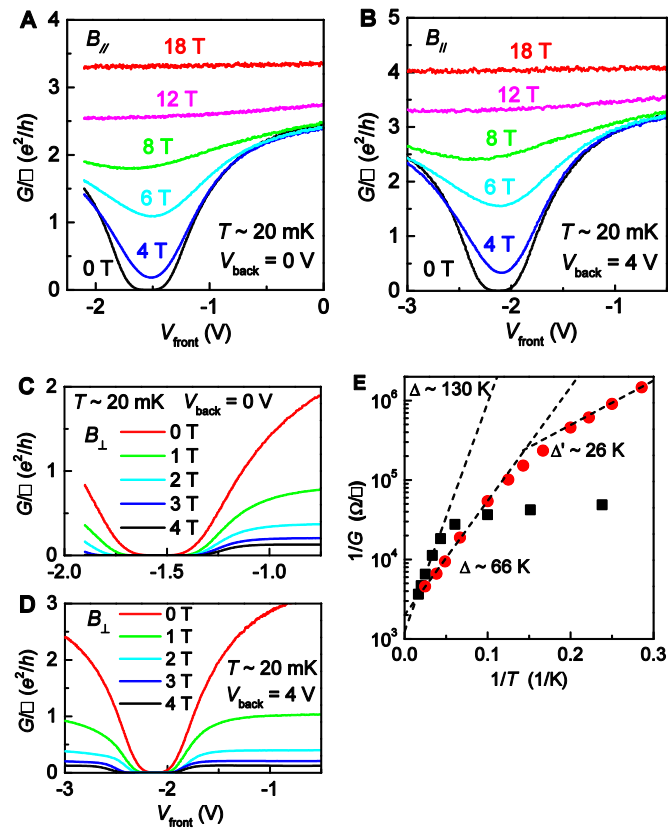


**Figure 2**

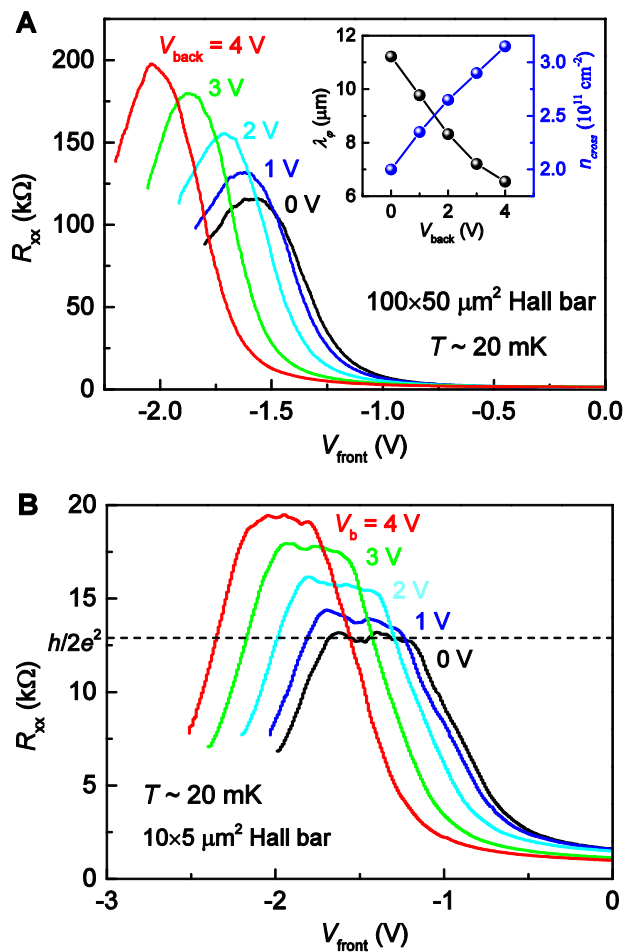


**Figure 3**

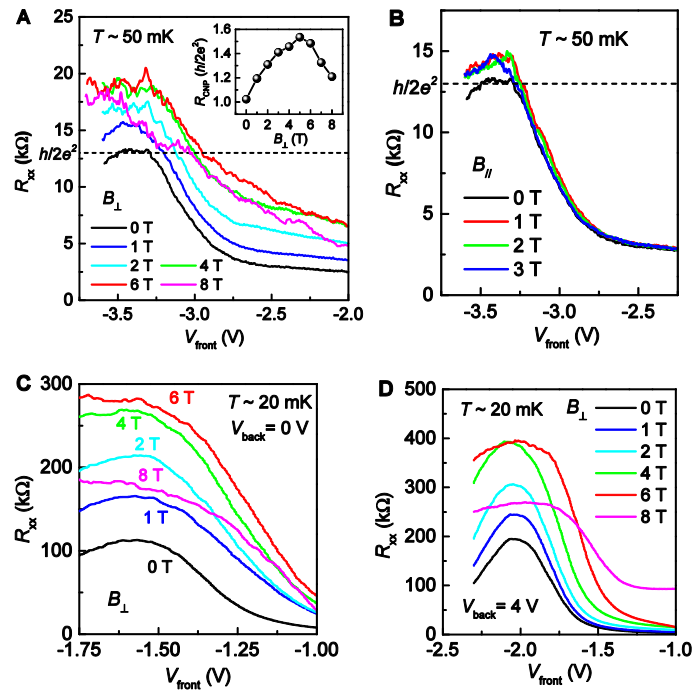


**Figure 4**

## Supplementary Information

### Strain-Engineering of InAs/GaInSb Topological Insulator Towards Majorana Platform

Lingjie Du<sup>1†</sup>, Tingxin Li<sup>1, 2, 4†</sup>, Wenkai Lou<sup>3</sup>, Xingjun Wu<sup>2, 4</sup>, Xiaoxue Liu<sup>2, 4</sup>, Zhongdong Han<sup>2, 4</sup>, Chi Zhang<sup>2, 4</sup>, Gerard Sullivan<sup>5</sup>, Amal Ikhlassi<sup>5</sup>, Kai Chang<sup>3</sup>, and Rui-Rui Du<sup>1, 2, 4\*</sup>

<sup>†</sup> These authors contributed equally to the project

\* Correspondent author: Rui-Rui Du at [rrd@rice.edu](mailto:rrd@rice.edu)

<sup>1</sup>Department of Physics and Astronomy, Rice University, Houston, Texas 77251-1892, USA

<sup>2</sup>International Center for Quantum Materials, School of Physics, Peking University, Beijing 100871, China

<sup>3</sup>SKLSM, Institute of Semiconductors, Chinese Academy of Sciences, Beijing 100083, China

<sup>4</sup>Collaborative Innovation Center of Quantum Matter, Beijing 100871, China

<sup>5</sup>Teledyne Scientific and Imaging, Thousand Oaks, California 91603, USA

## I Wafer characterizations

The semiconductor wafer of InAs/Ga<sub>0.75</sub>In<sub>0.25</sub>Sb QWs was grown by MBE technique. Fig. S1 shows the  $R_{xx}$ - $V_{\text{front}}$  trace and  $B/eR_{xy}$ - $V_{\text{front}}$  trace of a 30  $\mu\text{m} \times 10 \mu\text{m}$  Hall bar device measured at  $T \sim 50 \text{ mK}$ ,  $V_b = 0$ , and  $B_{\perp} = 2 \text{ T}$ . It can be seen that there is a singularity of  $B/eR_{xy}$ , corresponding to  $R_{xy} = 0$ . Based on the classical two-carrier transport model, the Hall resistance  $R_{xy}$  is given as:

$$R_{xy} = \frac{B[(p\mu_h^2 - n\mu_e^2) + \mu_e^2\mu_h^2 B^2(p - n)]}{e[(n\mu_e + p\mu_h)^2 + \mu_e^2\mu_h^2 B^2(p - n)^2]} \quad (1)$$

where  $n$  and  $p$  are electron and hole densities, and  $\mu_e$  and  $\mu_h$  are electron and hole mobilities, respectively;  $B$  is the perpendicular magnetic field. Therefore,  $R_{xy} = 0$  happens for the case  $p > n$ , since the  $\mu_h$  is lower than the  $\mu_e$ , while  $R_{xx}$  peak value appears when  $p = n \neq 0$ , thus the singularity of  $R_{xy}$  should be on the left of the  $R_{xx}$  peak, as shown in Fig. S1. On the other hand, if the bulk band is non-inverted, i.e. single carrier regime, both  $R_{xy} = 0$  and  $R_{xx}$  peak value should emerge for the case  $p = n = 0$ . In conclusion, data shown in Fig S1 has confirmed that

the bulk band structure of the present InAs/Ga<sub>0.75</sub>In<sub>0.25</sub>Sb QWs is inverted.

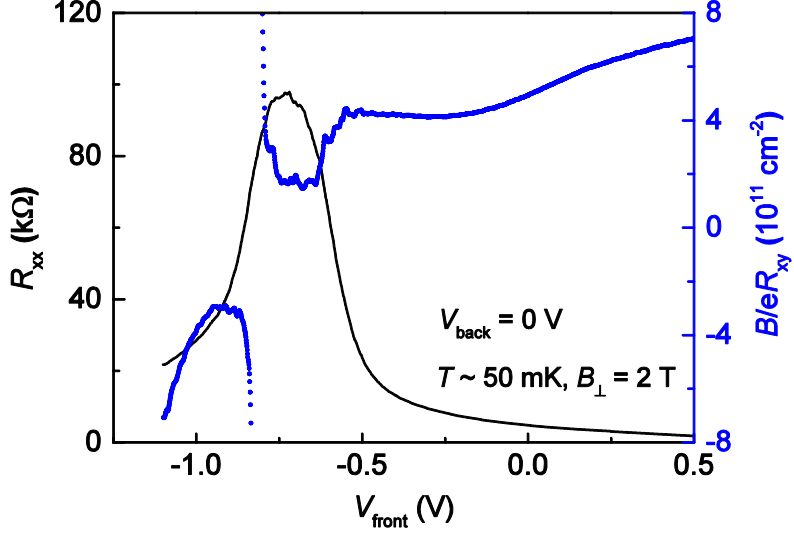


Figure S1:  $R_{xx}$ - $V_{\text{front}}$  trace and  $B/eR_{xy}$ - $V_{\text{front}}$  trace of a  $30 \mu\text{m} \times 10 \mu\text{m}$  Hall bar.

We note that for those samples having the band structures in the semiconductor gap regime, the  $R_{xy}$  should diverge near the edge of the gap, and consequently the  $B/eR_{xy}$  approaches  $0^+$  and  $0^-$ , respectively, as shown in ref. 6. Standard  $R_{xy}$  measurement should provide unambiguous identification distinguishing between the nontrivial gap in inverted band structure and trivial gap in semiconductor band.

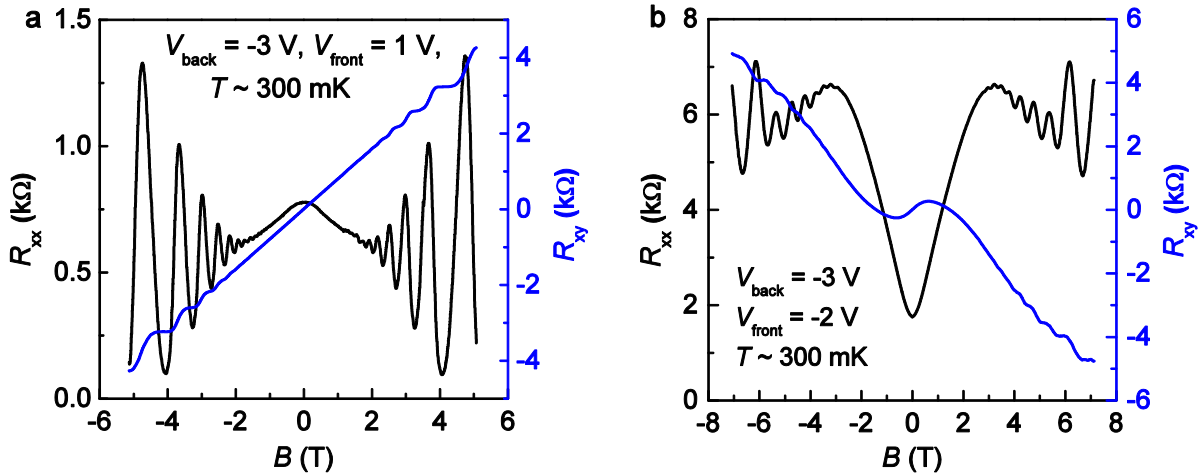


Figure S2: Magneto-transport data of the  $30 \mu\text{m} \times 10 \mu\text{m}$  Hall bar in **a**, electron-dominant regime and **b**, hole-dominant regime.

Figure S2a and S2b are two typical magneto-transport traces taken from the same device

shown in Fig. S1. Figure S2a is for the electron-dominant regime, where the electron density deduced from the SdH oscillations is  $\sim 7.8 \times 10^{11} \text{ cm}^{-2}$ , with mobility  $\sim 30,000 \text{ cm}^2/\text{Vs}$ . Figure S2b is for the hole-dominant regime. In addition, the  $R_{xy}$ - $B$  trace in Fig. S2b clearly shows deviations from linear-dependence, indicating the two-carrier transport regime.

## II More data of Corbino devices

Fig S3 shows  $G$ - $V_{\text{front}}$  traces of a Corbino device at different temperatures (below 500 mK). Although a large hybridization gap is formed in the strained InAs/Ga<sub>0.75</sub>In<sub>0.25</sub>Sb QWs, bulk is only truly insulating at very low temperatures. At  $\sim 500$  mK, the bulk resistance per square has already decreased to  $\sim 300$  k $\Omega$ .

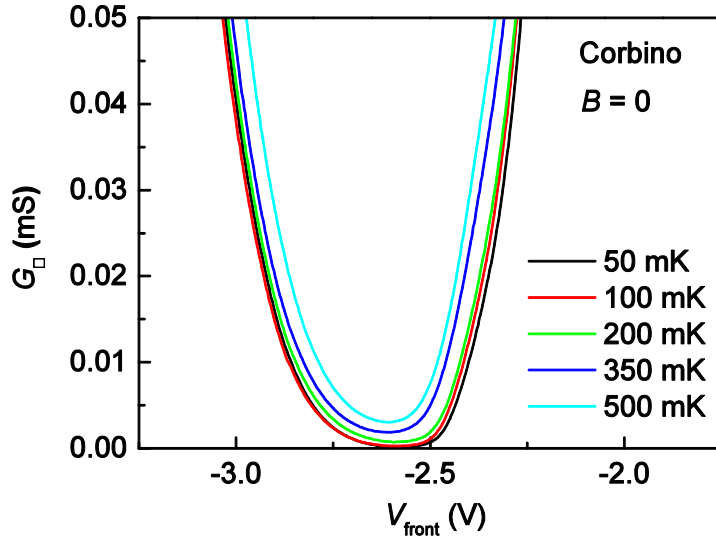


Figure S3:  $G$ - $V_{\text{front}}$  traces of a Corbino device at 50 mK, 100 mK, 200 mK, 350 mK, and 500 mK.

## III More data of magnetic field dependence for Hall bar devices

Fig. S4a and S4b show the  $R_{xx}$ - $V_{\text{front}}$  traces of the 100  $\mu\text{m} \times 50 \mu\text{m}$  Hall bar (mentioned in the main text) under in-plane magnetic field. It can be seen that the measured resistance peaks decrease, due to the bulk becoming conductive (semi-metallic) under  $B_{\parallel}$ .

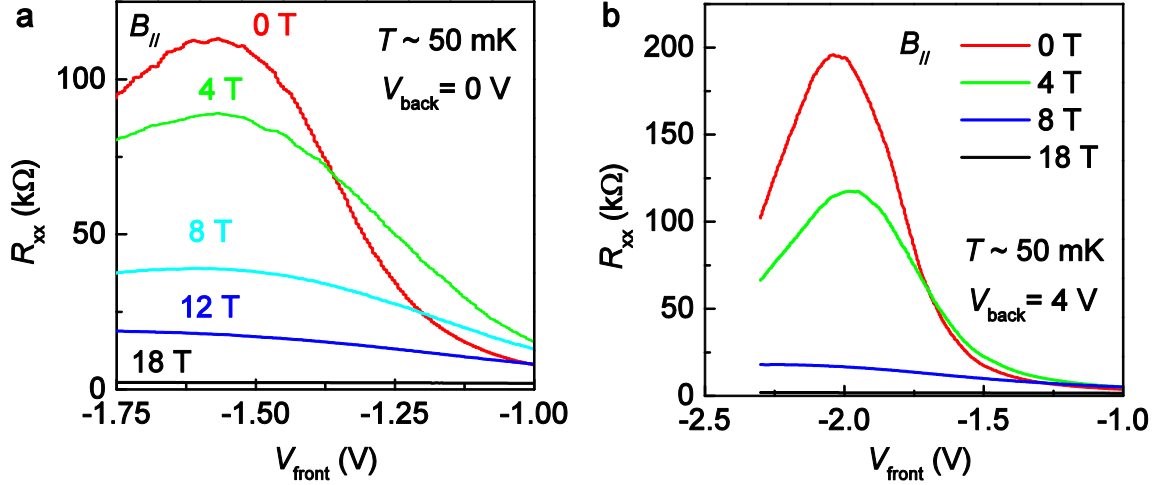


Figure S4:  $R_{xx}$ - $V_{\text{front}}$  traces of the  $100 \mu\text{m} \times 50 \mu\text{m}$  Hall bar under different in-plane magnetic field at  $V_{\text{back}} = 0 \text{ V}$  (shown in **a**) and  $V_{\text{back}} = 4 \text{ V}$  (shown in **b**), respectively.

Fig S5 shows the  $R_{\text{CNP}} - B_{\parallel}$  trace measured from a  $20 \mu\text{m} \times 10 \mu\text{m}$  Schottky gated Hall bar device. We hold the  $V_{\text{front}}$  at the  $R_{xx}$  peak during the measurements. Clearly, the measured resistance increase at first due to TRS breaking, then decrease because of bulk conductance.

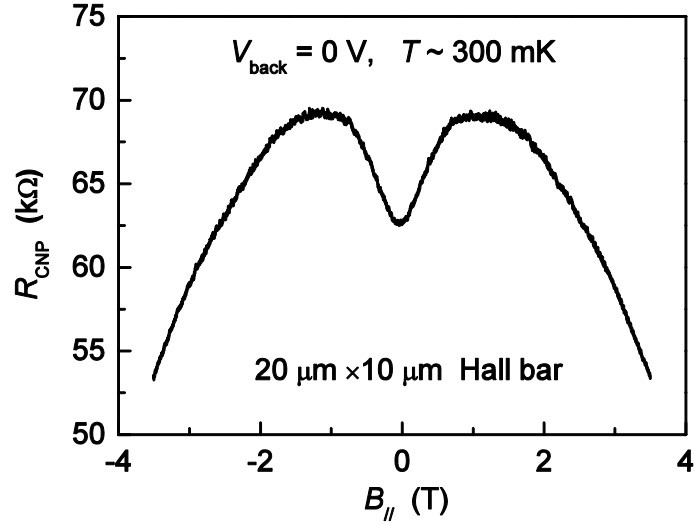


Figure S5:  $R_{\text{CNP}} - B_{\parallel}$  of a  $20 \mu\text{m} \times 10 \mu\text{m}$  Schottky gated Hall bar device, measured at  $300 \text{ mK}$ .